to treat (*28*). The fact that values of the diffusion coefficient (a fundamental descriptor of the dynamics) obtained from different experimental variables using 1D theories are similar suggests that these 1D descriptions of folding (*8*, *11*, *14*, *19*, *29*) can hold even at the microscopic level, despite their many simplifying assumptions.

The ability to observe and characterize transition paths opens up many exciting avenues to explore in folding studies by allowing more direct investigation of transition states and the microscopic thermally driven motions that underlie the conformational search. Previously invisible microstates along the transition paths may now be detectable, permitting their properties to be characterized directly. Moreover, it may be possible to distinguish different classes of transition paths having different properties, such as barrier heights, intermediates, or roughness. The potential for deeper integration of experiment and simulation through direct comparisons of the transition path properties found experimentally to the results of atomistic simulations is also exciting (*4*). Because the transit time is so sensitive to the diffusion coefficient D (*4*, *6*, *23*), such measurements also hold great promise for investigating the effects of solvent viscosity and internal friction (*4*, *6*, *30*).

REFERENCES AND NOTES

1. J. D. Bryngelson, P. G. Wolynes, *Proc. Natl. Acad. Sci. U.S.A.* **84**, 7524–7528 (1987).
2. J. Buchner, T. Kiefhaber, Eds., *Protein Folding Handbook* (Wiley-VCH, Weinheim, Germany, 2005).
3. P. G. Bolhuis, D. Chandler, C. Dellago, P. L. Geissler, *Annu. Rev. Phys. Chem.* **53**, 291–318 (2002).
4. H. S. Chung, S. Piana-Agostinetti, D. E. Shaw, W. A. Eaton, *Science* **349**, 1504–1510 (2015).
5. H. S. Chung, K. McHale, J. M. Louis, W. A. Eaton, *Science* **335**, 981–984 (2012).
6. H. S. Chung, W. A. Eaton, *Nature* **502**, 685–688 (2013).
7. H. S. Chung, J. M. Louis, W. A. Eaton, *Proc. Natl. Acad. Sci. U.S.A.* **106**, 11837–11844 (2009).
8. K. Truex, H. S. Chung, J. M. Louis, W. A. Eaton, *Phys. Rev. Lett.* **115**, 018101 (2015).
9. D. B. Ritchie, M. T. Woodside, *Curr. Opin. Struct. Biol.* **34**, 43–51 (2015).
10. K. Neupane *et al.*, *Phys. Rev. Lett.* **109**, 068102 (2012).
11. H. Yu *et al.*, *Proc. Natl. Acad. Sci. U.S.A.* **109**, 14452–14457 (2012).
12. M. T. Woodside, S. M. Block, *Annu. Rev. Biophys.* **43**, 19–39 (2014).
13. R. B. Best, G. Hummer, *Proc. Natl. Acad. Sci. U.S.A.* **102**, 6732–6737 (2005).
14. K. Neupane, A. P. Manuel, J. Lambert, M. T. Woodside, *J. Phys. Chem. Lett.* **6**, 1005–1010 (2015).
15. M. T. Woodside *et al.*, *Proc. Natl. Acad. Sci. U.S.A.* **103**, 6190–6195 (2006).
16. M. T. Woodside *et al.*, *Science* **314**, 1001–1004 (2006).
17. A. N. Gupta *et al.*, *Nat. Phys.* **7**, 631–634 (2011).
18. M. C. Engel, D. B. Ritchie, D. A. N. Foster, K. S. D. Beach, M. T. Woodside, *Phys. Rev. Lett.* **113**, 238104 (2014).
19. A. P. Manuel, J. Lambert, M. T. Woodside, *Proc. Natl. Acad. Sci. U.S.A.* **112**, 7183–7188 (2015).
20. Materials and methods are available as supplementary materials on *Science* Online.
21. S. Chaudhury, D. E. Makarov, *J. Chem. Phys.* **133**, 034118 (2010).
22. P. Hänggi, P. Talkner, M. Borkovec, *Rev. Mod. Phys.* **62**, 251–341 (1990).
23. M. T. Woodside, J. Lambert, K. S. D. Beach, *Biophys. J.* **107**, 1647–1653 (2014).
24. G. Hummer, *J. Chem. Phys.* **120**, 516–523 (2004).
25. H. Yu *et al.*, *Proc. Natl. Acad. Sci. U.S.A.* **112**, 8308–8313 (2015).
26. M. Hinczewski, Y. von Hansen, R. R. Netz, *Proc. Natl. Acad. Sci. U.S.A.* **107**, 21493–21498 (2010).
27. P. Cossio, G. Hummer, A. Szabo, *Proc. Natl. Acad. Sci. U.S.A.* **112**, 14248–14253 (2015).
28. G.-M. Nam, D. E. Makarov, *Protein Sci.* **25**, 123–134 (2016).
29. W. Zheng, R. B. Best, *J. Phys. Chem. B* **119**, 15247–15255 (2015).
30. A. Borgia *et al.*, *Nat. Commun.* **3**, 1195 (2012).

ACKNOWLEDGMENTS

We thank D. Makarov and A. Szabo for helpful discussions. This work was supported by the Alberta Prion Research Institute, Alberta Innovates (AI) Technology Futures, AI Health Solutions, the Natural Sciences and Engineering Research Council, and National Research Council Canada. M.T.W., K.N., and D.R.D. designed the research; F.W. provided new reagents; K.N., D.A.N.F., and H.Y. performed measurements; K.N., D.R.D., and M.T.W. analyzed the data; and M.T.W., K.N., D.R.D., D.A.N.F., and H.Y. wrote the paper.

SUPPLEMENTARY MATERIALS

www.sciencemag.org/content/352/6282/239/suppl/DC1
Materials and Methods
Fig. S1
References (*31*–*36*)

20 July 2015; accepted 18 February 2016
10.1126/science.aad0637

CANCER

SCS macrophages suppress melanoma by restricting tumor-derived vesicle–B cell interactions

Ferdinando Pucci,[1]* Christopher Garris,[1,2] Charles P. Lai,[3]† Andita Newton,[1] Christina Pfirschke,[1] Camilla Engblom,[1,2] David Alvarez,[4] Melissa Sprachman,[1] Charles Evavold,[1,2] Angela Magnuson,[1] Ulrich H. von Andrian,[4] Katharina Glatz,[5] Xandra O. Breakefield,[3] Thorsten R. Mempel,[6] Ralph Weissleder,[1] Mikael J. Pittet[1]‡

Tumor-derived extracellular vesicles (tEVs) are important signals in tumor–host cell communication, yet it remains unclear how endogenously produced tEVs affect the host in different areas of the body. We combined imaging and genetic analysis to track melanoma-derived vesicles at organismal, cellular, and molecular scales to show that endogenous tEVs efficiently disseminate via lymphatics and preferentially bind subcapsular sinus (SCS) CD169$^+$ macrophages in tumor-draining lymph nodes (tdLNs) in mice and humans. The CD169$^+$ macrophage layer physically blocks tEV dissemination but is undermined during tumor progression and by therapeutic agents. A disrupted SCS macrophage barrier enables tEVs to enter the lymph node cortex, interact with B cells, and foster tumor-promoting humoral immunity. Thus, CD169$^+$ macrophages may act as tumor suppressors by containing tEV spread and ensuing cancer-enhancing immunity.

Although cancer is driven by tumor cell–endogenous genetic mutations, it is also modulated by tumor cell–exogenous interactions with host components, including immune cells (*1*). Tumor-induced host immune system activation can occur both within and away from the tumor stroma and may involve different communication signals, including soluble factors (*2*) and tumor-derived extracellular vesicles (tEVs) (*3*). tEVs are key candidate conveyors of information between cancer and host immune cells because they can travel long distances in the body without their contents degrading or diluting. tEVs may transfer surface receptors or intracellular material to different host acceptor cells (*4*–*6*); these processes have all been associated with altered antitumor immunity and enhanced cancer progression (*7*). Circulating tEVs also have diagnostic and prognostic potential, as they can be used to detect early cancer stages (*8*) and to predict overall patient survival (*4*) and treatment responses (*9*). Despite increased understanding of tEVs' importance, a critical barrier to progress in the field has been our limited ability to assess the impact of vesicles that are produced in vivo (*7*). To shift current experimental research on tEV–host cell interactions, we combined imaging and genetic approaches to track endogenously produced tEVs and their targets at different resolutions and scales.

We assessed the whole-body biodistribution of tumor-derived material in mice bearing genetically modified B16F10 melanoma tumors (B16F10-mGluc), which produce tEVs carrying membrane-bound *Gaussia* luciferase (mGluc) (*10*) (fig. S1). Quantification of tEV-bound mGluc activity in various

[1]Center for Systems Biology, Massachusetts General Hospital Research Institute, Harvard Medical School, Boston, MA 02114, USA. [2]Graduate Program in Immunology, Harvard Medical School, Boston, MA 02115, USA. [3]Department of Neurology, Massachusetts General Hospital Research Institute, Harvard Medical School, Charlestown, MA 02129, USA. [4]Department of Microbiology and Immunobiology, Harvard Medical School, Boston, MA 02115, USA. [5]Institute of Pathology, University Hospital Basel, 4031 Basel, Switzerland. [6]Center for Immunology and Inflammatory Diseases, Massachusetts General Hospital Research Institute, Harvard Medical School, Charlestown, MA 02129, USA.
*Present address: Torque Therapeutics Inc., Cambridge, MA 02142, USA. †Present address: Institute of Biomedical Engineering, National Tsing Hua University, Hsinchu, Taiwan. **‡Corresponding author. E-mail: mpittet@mgh.harvard.edu**

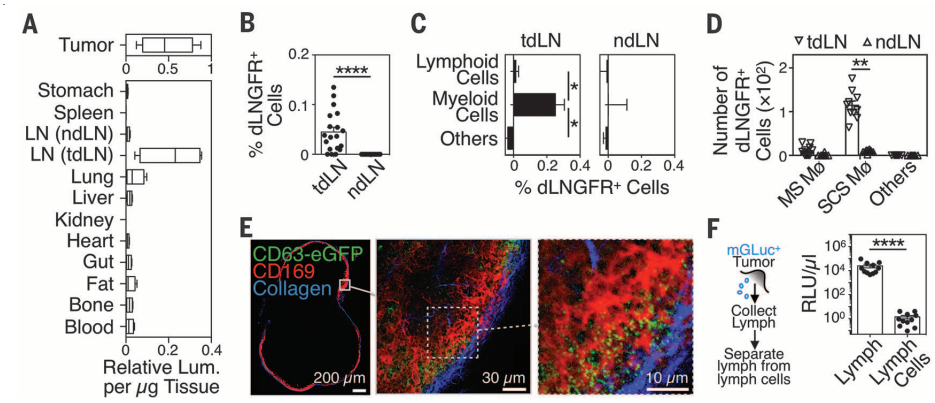

Fig. 1. Endogenous tEVs disseminate via lymph and interact with tumor-draining LN SCS macrophages. (**A**) Relative mGLuc luminescence activity (per microgram of tissue) in various organs isolated from mice carrying B16F10-mGLuc$^+$ melanoma tumors on week 2 after tumor challenge (two independent experiments, $n = 8$ to 10). (**B** to **E**) Quantification of host dLNGFR$^+$ cells in (B) total tdLN and ndLN cells, (C) lymphoid/myeloid cell fractions, and (D) macrophage subsets isolated from mice carrying dLNGFR$^+$ B16F10 melanoma tumors on week 2 after tumor challenge (two independent experiments, $n > 10$). (E) Representative multiphoton micrographs of an explanted tdLN from a mouse carrying CD63-eGFP$^+$ B16F10 melanoma on week 2 after tumor challenge (two independent experiments, $n = 6$). (**F**) Experimental outline of lymph collection (left) and quantification of mGLuc signal in cell-free lymph and cells from lymph (two independent experiments; $n = 11$). $^{**}P < 0.01$, $^{****}P < 0.0001$ (Mann-Whitney test). Lum, luminescence; Mø, macrophage; MS, medullary sinus; ndLN, non–tumor-draining LN; TAM, tumor-associated macrophages; tdLN, tumor-draining LN.

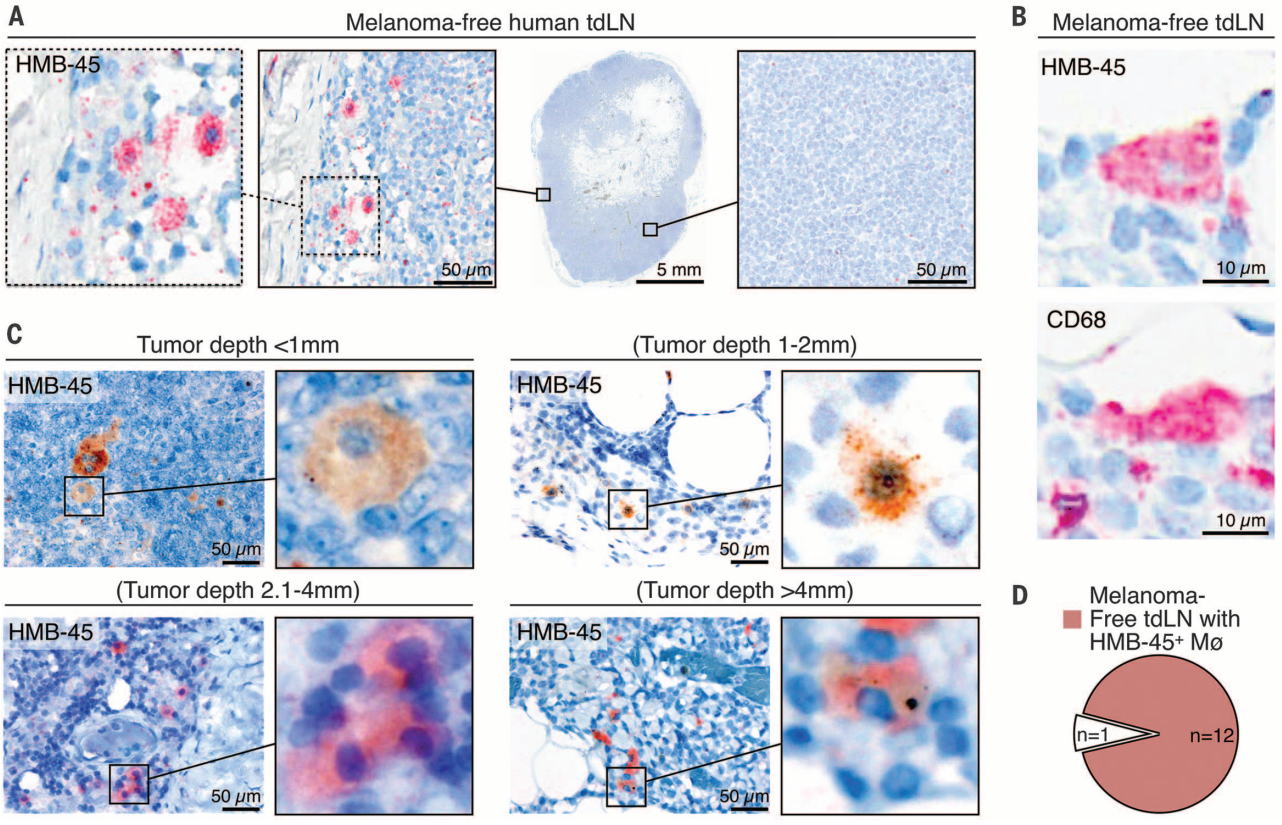

Fig. 2. Human SCS macrophages collect tumor-derived materials in melanoma-free tumor-draining LNs. (**A**) Immunohistochemistry for the melanoma marker HMB-45 (red) in a tdLN from a melanoma-free (i.e., stage N0) patient. The tissue was counterstained with hematoxylin (blue). (**B**) Immunohistochemistry for HMB-45 melanoma (top) and CD68 macrophage markers (bottom) in sequential sections from a melanoma-free (i.e., stage N0) tdLN. (**C**) HMB-45 immunohistochemistry (brown or red) in tdLNs from melanoma-free patients with different tumor stages (according to American Joint Committee on Cancer guidelines). Primary tumor depth is indicated above each image. Tissues were counterstained with hematoxylin (blue). (**D**) Pie chart illustrating the fraction of patients containing HMB-45$^+$ macrophages in melanoma-free tdLNs.

tissues from B16F10-mGLuc$^+$ tumor-bearing mice not only confirmed that B16F10-mGLuc$^+$–derived tEVs can exit the tumor stroma and relocate to remote organs but also identified the highest relative mGLuc activity in tumor-draining lymph nodes (tdLNs) when compared to blood, spleen, bone, lung, liver, non–tumor-draining LNs (ndLNs), and other tissues (Fig. 1A and fig. S2A). Consistently, we measured higher mGLuc signal in lymph than in plasma (fig. S2B). Control tumors expressing secreted *Gaussia* luciferase (sGLuc) did not generate bioluminescence activity in tdLNs (fig. S2C).

To decipher endogenous tEVs' interactions in tdLNs at the cellular level, we investigated mice bearing genetically modified B16F10 melanoma cells expressing two membrane-bound reporters: the vesicular membrane-associated protein CD63 fused with enhanced green fluorescent protein (CD63-eGFP), and the ubiquitous transmembrane marker dLNGFR (truncated receptor for nerve growth factor) (fig. S3). Flow cytometry–based analyses revealed dLNGFR$^+$ cells in tdLNs but not in ndLNs (Fig. 1B). These tdLNs did not include tumor cells or tumor cell apoptotic bodies

(figs. S4 to S6). The dLNGFR signal originated mostly from myeloid cells, not lymphoid cells (Fig. 1C). Among tdLN myeloid cells, the CD11b$^+$ side scatter–low fraction, which resembles subcapsular sinus (SCS) macrophages (*11*), was dLNGFR$^+$, whereas CD11b$^+$ SSC^{HI} marginal sinus macrophages remained largely dLNGFR$^-$ (Fig. 1D and fig. S7). Multiphoton microscopy and three-dimensional reconstructions of tEV distribution confirmed CD169$^+$ SCS macrophages as a major host cell type interacting with CD63-eGFP$^+$ tEVs in vivo (Fig. 1E and figs. S8 and S9). The vesicles accumulated principally between 10 and 20 μm below the LN capsule and adjacent to CD169$^+$ SCS macrophages, which occupy the space between 20 and 80 μm below the capsule.

We asked whether CD169$^+$ SCS macrophages originate from the tumor stroma, where they may initially capture tEVs. B16F10 tumors were implanted in mice ubiquitously expressing the photoconvertible protein Kaede (*12*), and the tumor site was exposed to ultraviolet light in order to shift Kaede fluorescence emission from green to red selectively in tumor-infiltrating host cells (fig. S10, A and B). The tdLN SCS macrophages remained green 24 hours later and therefore did not originate from the tumor stroma (fig. S10C). Photoconverted cells in tdLNs were mostly CD103$^+$ DCs (fig. S10D). These migratory cells might not be involved in carrying tEVs to LNs, because analysis of lymph collected from B16F10-mGLuc tumor-bearing mice revealed mGLuc activity that was higher by a factor of >10^4 in cell-free fractions than in cells from lymph (Fig. 1F). These data suggest that tEVs freely disseminate to tdLNs, where they preferentially bind resident SCS macrophages.

To define our findings' relevance for human disease, we examined cancer-free sentinel LN (CF-SLN) biopsies from 13 melanoma patients (table S1). Melanin pigment staining was found selectively in macrophage-like populations (figs. S11 and S12, A to C). We then assessed melanoma-derived material by staining CF-SLNs with the monoclonal antibody (mAb) clone HMB-45, which is used to pathologically evaluate melanoma metastasis in regional SLNs. HMB-45 reacts with a transmembrane glycoprotein that is part of the gp100 pre-melanosome complex and is expressed by >80% of melanomas (*13*). Although the SLNs analyzed were melanoma-free (i.e., stage N0), we identified HMB-45$^+$ cells that corresponded to macrophages morphologically and resided mostly near the LN capsule (Fig. 2A and fig. S12D). Serial staining of CF-SLN sections for HMB-45 and the macrophage marker CD68 confirmed that the observed HMB-45$^+$ cells were CD68$^+$ macrophages (Fig. 2B and fig. S13). To interrogate the temporal course of HMB-45$^+$ signal appearance during melanoma progression, we assessed CF-SLNs from patients with distinct clinical stages based on Breslow's thickness (tumor depths ranging from <1 mm to >4 mm). We identified HMB-45$^+$ macrophages in >90% of patients independent of tumor progression (Fig. 2, C and D), which suggests that melanoma-derived material reaches SLNs early in cancer progression, similar to our observations in mice (fig. S14).

Given that EVs can deliver intracellular RNAs and proteins into target cells and that horizontal transfer can shape the fate of acceptor cells (*4*–*6*), we asked whether such transfer characterizes SCS macrophage–tEV interactions. We used transgenic mice that express yellow fluorescent protein (YFP) upon Cre-mediated recombination and challenged these mice with genetically modified B16F10 melanoma tumor cells expressing Cre (fig. S15, A to E). Fusion of Cre$^+$ tEVs with host acceptor cells would irreversibly induce YFP

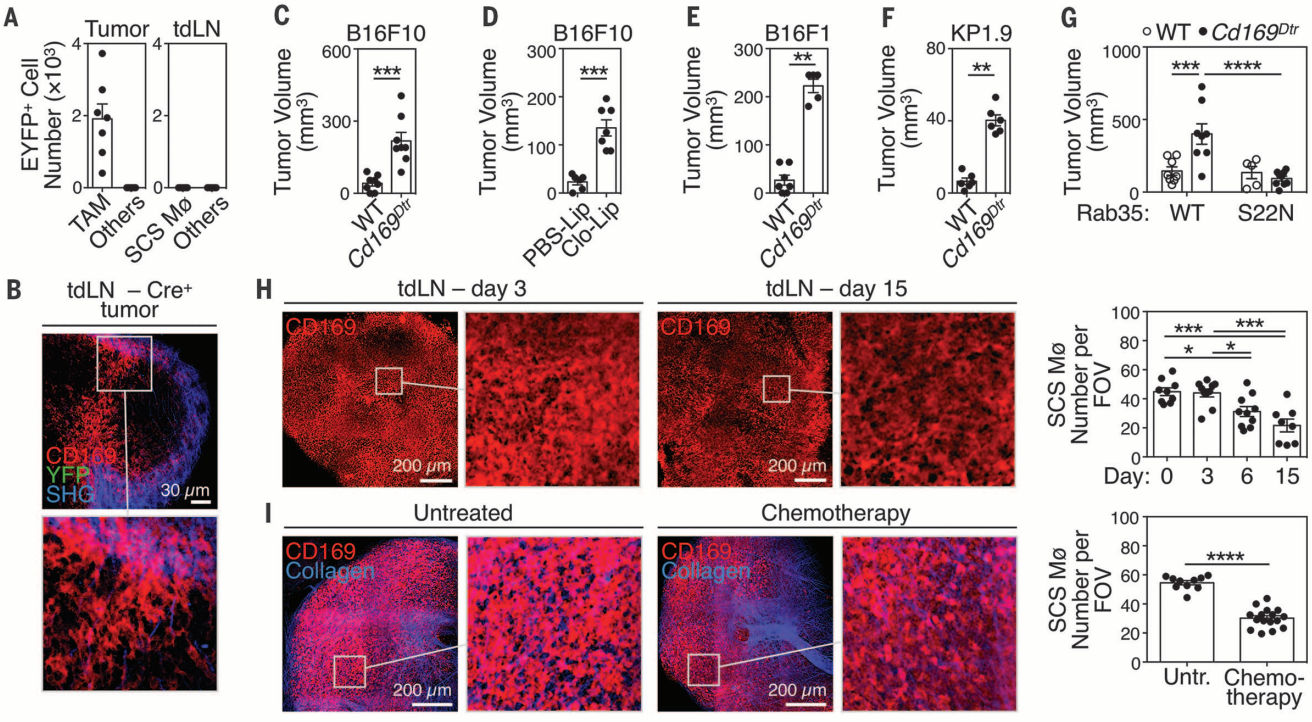

Fig. 3. SCS macrophage–tEV interactions suppress tumor growth. (**A**) Number of eYFP$^+$ TAMs, SCS macrophages, and other cells on week 2 after challenging Cre-reporter mice with Cre$^+$ B16F10 tumors (two independent experiments, n = 7). (**B**) Multiphoton micrographs of LNs draining Cre$^+$ tumors (one experiment, n = 3). (**C**) B16F10 tumor volume in wild-type or *Cd169*$^{Dtr/Wt}$ mice, all treated with DT intraperitoneally (i.p.; two independent experiments, n = 8). (**D**) B16F10 tumor volume in wild-type mice treated with phosphate-buffered saline (PBS)–Lip or Clo-Lip subcutaneously (s.c.; two independent experiments; n = 6 or 7). (**E**) B16F1 melanoma tumor volume in wild-type or *Cd169*$^{Dtr/Wt}$ mice, all treated with DT i.p. (n = 5 to 7). (**F**) KP1.9 lung adenocarcinoma tumor volume in wild-type or *Cd169*$^{Dtr/Wt}$ mice, all treated with DT i.p. (n = 6). (**G**) B16F10 tumor volume in wild-type or *Cd169*$^{Dtr/Wt}$ mice, all treated with DT i.p., and challenged with tumors expressing either Rab35^{WT} or Rab35^{S22N} (n = 5 to 8). (**H**) Left: multiphoton micrographs (2D projections of 30 high-resolution optical sections spanning the whole LN with 2 μm Z-spacing) of tdLNs on day 3 and 15 after B16F10 tumor challenge (n = 2 or 3). Right: Quantification of SCS macrophage barrier disruption measured as CD169$^+$ SCS macrophage number per field of view. (**I**) Left: Multiphoton micrographs [obtained similarly as in (H)] of inguinal LNs 1 week after starting i.p. paclitaxel/carboplatin injections, 3 times per week (n = 4). Right: quantification as in (H). *P < 0.05, **P < 0.01, ***P < 0.001, ****P < 0.0001 [Mann-Whitney test for (C), (D), (E), (F), and (I); two-way analysis of variance (ANOVA) for (G); one-way ANOVA with Tukey's multiple comparisons test for (H)]. Clo-Lip, clodronate-loaded liposomes; DT, diphtheria toxin; FOV, field of view; PBS-Lip, PBS-loaded liposomes; Untr., untreated.

expression in the target cell. Analysis of B16F10-Cre^{+} tumor-bearing mice identified Cre-induced YFP expression in tumor-associated macrophages (TAMs); however, tdLN CD169^{+} SCS macrophages (and all other tdLN cells) remained exclusively YFP^{-} (Fig. 3, A and B, and fig. S15F). Thus, on their own, endogenous tEVs are unlikely to modulate SCS macrophages through horizontal transfer.

Because SCS macrophage–tEV interactions may regulate tumor progression independently from horizontal transfer, we assessed whether modulating SCS macrophages and/or tEVs affects cancer growth in vivo. We examined *Cd169*$^{Dtr/Wt}$ knock-in mice in which CD169^{+} LN macrophages were specifically depleted by diphtheria toxin (DT) injection (figs. S16 and S17). CD169^{+} LN macrophage removal significantly enhanced B16F10 tumor growth (Fig. 3C). Similarly, specifically depleting CD169^{+} LN macrophages by subcutaneous administration of clodronate liposomes (figs. S18 and S19) accelerated B16F10 tumor progression in wild-type mice (Fig. 3D). Thus, CD169^{+} LN macrophages act as "tumor suppressors" in orthotopic B16F10 melanoma; these findings were extended to orthotopic B16F1 melanoma (Fig. 3E) and KP lung adenocarcinoma (Fig. 3F).

To assess whether interactions between endogenous tEVs and SCS macrophages affect tumor progression, we introduced a single copy of either Rab35 wild-type (Rab35^{WT}) or Rab35 dominant-negative Ser^{22} → Asn mutant (Rab35^{S22N}) (*14*) into B16F10 melanoma cells. These tumors had normal or impaired capacity, respectively, to release tEVs (fig. S20). As expected, removing CD169^{+} macrophages accelerated B16F10 Rab35^{WT} tumor progression; however, Rab35^{S22N} tumors grew similarly with or without CD169^{+} macrophages (Fig. 3G). The observation that enhanced tumor growth from SCS macrophage ablation only occurs in the context of sufficient tEV production supports a causal link between SCS macrophage–tEV interaction and tumor growth.

We then asked whether cancer disrupts SCS macrophage network organization, because pathogens entering LNs can induce such alterations (*15*). Three-dimensional multiphoton imaging of tdLNs revealed a decrease in CD169^{+} SCS macrophage density as soon as day 6 after tumor challenge (Fig. 3H). This may happen because tdLNs enlarge without expanding their SCS macrophage pool, as indicated by photoconversion (fig. S10), parabiosis (fig. S21A), 5-bromo-2′-deoxyuridine (BrdU; fig. S21B), and Ki67 labeling studies (fig. S21C). These results imply different ontogenesis for TAMs and SCS macrophages because, unlike SCS macrophages, most TAMs derive from circulating monocytes and can divide in some tumors (*16*, *17*). Chemotherapy with paclitaxel and carboplatin (Fig. 3I) and immunotherapy with a small-molecule CSF-1R inhibitor (fig. S22) also reduced CD169^{+} SCS macrophage density. Thus, the SCS macrophage barrier can be disrupted both during the natural course of tumor progression and upon anticancer treatment.

Because SCS macrophage–tEV interactions are geographically restricted to tdLNs, yet modulate the outgrowth of distant tumors, they may influence a systemic response to cancer. Indeed, depletion of CD169^{+} tdLN macrophages on one side only (fig. S23) was sufficient to accelerate both contralateral and ipsilateral tumor growth (Fig. 4A). We hypothesized that tEVs may bind and regulate discrete host components upon disruption of the SCS macrophage layer. Interestingly, tdLN multiphoton imaging revealed that, without SCS macrophages, tEVs efficiently penetrated the LN cortex (Fig. 4B). These findings indicate that SCS macrophages act as tEV gatekeepers—a capacity that resembles these macrophages' ability to prevent the systemic spread of lymph-borne pathogens (*15*, *18*–*20*).

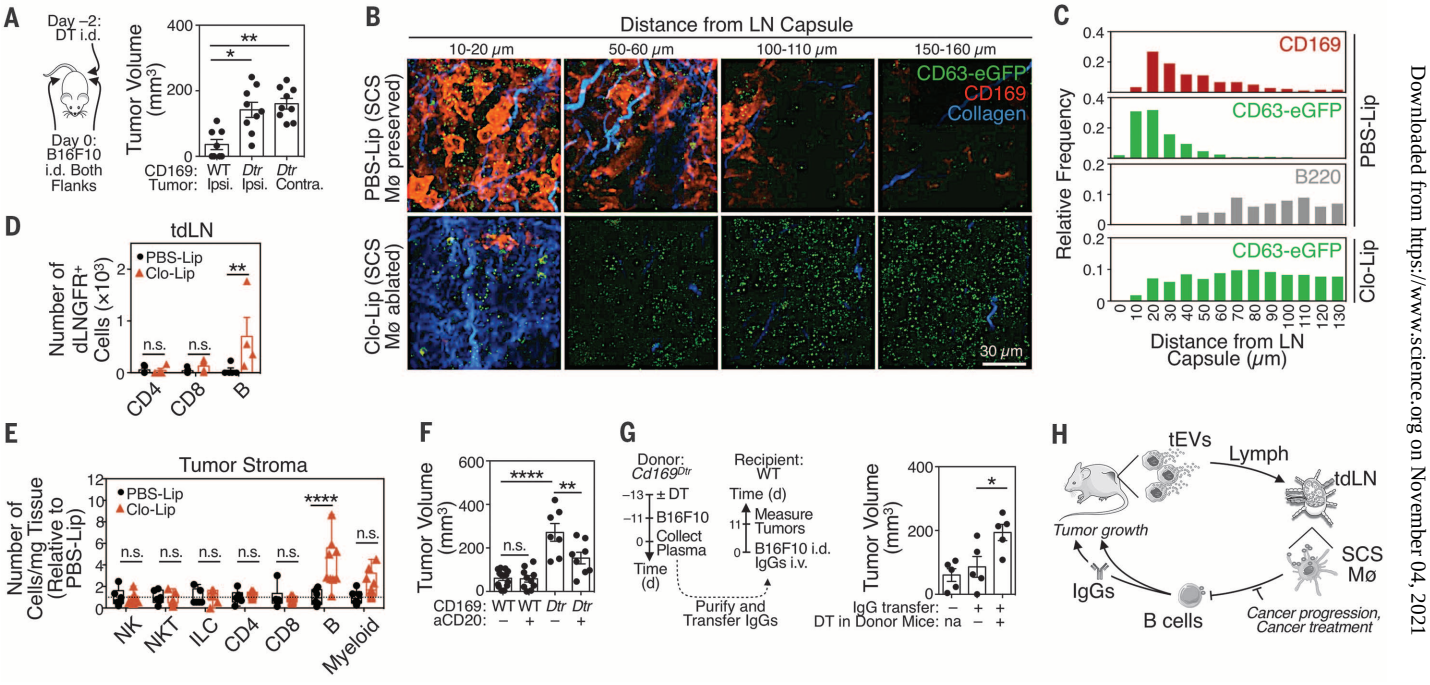

Fig. 4. SCS macrophage–tEV interactions suppress tumor-promoting B cell immunity. (**A**) Tumor volumes in *Cd169*$^{Dtr/Wt}$ mice locally treated with DT intradermally (i.d.) on one side and challenged with B16F10 tumors on both flanks i.d. (n = 9). (**B**) Multiphoton micrographs of tdLNs from CD63-eGFP^{+} B16F10 tumor-bearing mice (treated with PBS-Lip or Clo-Lip s.c.) and imaged at the indicated depth below the LN capsule (blue). Red, CD169; green, eGFP (two independent experiments, n = 3). (**C**) Distance between the indicated entities (CD169^{+} cells, CD63-eGFP^{+} tEVs, and B220^{+} cells) and the LN capsule, plotted as relative frequency versus position. (**D**) Flow cytometry–based quantification of dLNGFR^{+} lymphocyte subsets in tdLNs from dLNGFR^{+} B16F10 melanoma-bearing mice treated with PBS-Lip or Clo-Lip s.c. (n = 4 or 5). (**E**) Flow cytometry–based quantification of different cell types in B16F10 tumors from mice treated with PBS-Lip or Clo-Lip (data are normalized to PBS-Lip–treated mice; two independent experiments, n = 9). (**F**) B16F10 tumor volumes (day 9) in wild-type and *Cd169*$^{Dtr/Wt}$ mice treated with DT i.p. and/or with CD20-depleting mAb (n = 7 to 10). (**G**) B16F10 tumor volumes in wild-type recipient mice that received IgGs (25 μg) isolated from plasma of *Cd169*$^{Dtr/Wt}$ donor mice treated with PBS or DT i.p. (n = 5). Mice that did not receive IgGs were used as controls. (**H**) Proposed model. *P < 0.05, **P < 0.01, ****P < 0.0001; n.s., not significant. Kruskal-Wallis test with Dunn's multiple comparisons test for (A); two-way ANOVA with Sidak's multiple comparisons test for (D) and (E); one-way ANOVA with Tukey's multiple comparisons test for (F) and (G). aCD20, CD20 mAb; Contra, contralateral; DTR, DT receptor; ILC, innate lymphoid cells; Ipsi, ipsilateral; NK, natural killer cells; NKT, natural killer T cells.

Multiphoton imaging of tdLNs in SCS macrophage–depleted mice further revealed that tEVs reached B cell follicles (Fig. 4C). Also, flow cytometry–based analysis of tdLNs identified B cells as the only detectable immune population physically interacting with tEVs in these mice (Fig. 4D and fig. S24A). Such interaction was lost in mice bearing Rab35S22N tumors, which are impaired to secrete tEVs (fig. S24B). B cells remained YFP^- in tdLNs from B16F10-Cre^+ tumor-bearing Cre-reporter mice treated with clodronate liposomes, indicating that tEV horizontal gene transfer to B cells does not occur in the absence of SCS macrophages (fig. S24A). However, various B cell subsets increased in tdLNs, and concomitantly decreased in ndLNs, as tumors progressed (fig. S24, C and D). The concentration of tumor-infiltrating B cells also increased by a factor of ~3 in SCS macrophage–depleted mice, whereas other immune cell populations remained detectably unchanged (Fig. 4E and fig. S25). To test a causal role for B cells in enhancing melanoma growth after $CD169^+$ LN macrophage ablation, we removed B cells by means of a CD20 mAb in DT-treated *Cd169*$^{Dtr/Wt}$ mice. B cell ablation significantly decreased tumor progression in this experimental setting (Fig. 4F). These data imply that B cells are tumor-promoting cells through tEV–B cell interactions that can be suppressed by SCS macrophages.

Because B cells may foster tumor progression by producing autoantibodies (*21*–*23*), we tested whether manipulating SCS macrophages modulates immunoglobulin G (IgG) responses. Indeed, $CD169^+$ LN macrophage depletion amplified tdLN plasma cells (fig. S26A) and increased both plasma IgG concentration (fig. S26B) and IgG affinity for tumor antigens (fig. S26C). The increased IgG concentration required full-fledged tEV secretion by tumors (fig. S26D). Most important, transfer of circulating IgGs from B16F10 tumor-bearing mice, in which SCS macrophages were depleted, significantly accelerated tumor growth in SCS macrophage–competent mice (Fig. 4G and fig. S27). Thus, SCS macrophages can suppress cancer progression at least partly by limiting pro-tumor IgG responses (Fig. 4H).

Our study identifies SCS macrophages as tumor-suppressive cells, in contrast to TAMs that often display tumor-promoting activities (*24*). Yet tumor progression and at least some therapeutic agents undermine the SCS macrophage barrier, thereby enabling tEV interaction with B cells in the LN cortex and activating tumor-enhancing B cell immunity. Previous studies that investigated acute responses to pathogens and model foreign antigens had established that SCS macrophages can promote B cell responses (*15*, *20*, *25*–*27*). The present data suggest that SCS macrophages can also provide a physical barrier to B cell activity under specific circumstances. It is possible that SCS macrophages acquire different functions when exposed continuously to inflammatory triggers or in the context of sterile inflammation. Additionally, tEVs may have unique properties that prevent their presentation by SCS macrophages to B cells or that alter SCS macrophage functions in vivo. Thus far, macrophage-targeting therapies to treat cancer are mostly aimed at depleting these cells indiscriminately (*28*). Instead, our results favor therapeutic approaches that limit harmful TAM functions while leaving SCS macrophages unaffected. Whether it is possible to selectively expand SCS macrophages to control cancer also deserves consideration. In support of this scenario, a high density of $CD169^+$ macrophages in regional LNs positively correlated with longer overall survival in patients with colorectal carcinoma (*29*).

REFERENCES AND NOTES

1. D. Hanahan, R. A. Weinberg, *Cell* **144**, 646–674 (2011).
2. S. S. McAllister, R. A. Weinberg, *Nat. Cell Biol.* **16**, 717–727 (2014).
3. M. Colombo, G. Raposo, C. Théry, *Annu. Rev. Cell Dev. Biol.* **30**, 255–289 (2014).
4. H. Peinado *et al*., *Nat. Med.* **18**, 883–891 (2012).
5. J. Skog *et al*., *Nat. Cell Biol.* **10**, 1470–1476 (2008).
6. A. Zomer *et al*., *Cell* **161**, 1046–1057 (2015).
7. F. Pucci, M. J. Pittet, *Clin. Cancer Res.* **19**, 2598–2604 (2013).
8. S. A. Melo *et al*., *Nature* **523**, 177–182 (2015).
9. H. Shao *et al*., *Nat. Commun.* **6**, 6999 (2015).
10. C. P. Lai *et al*., *ACS Nano* **8**, 483–494 (2014).
11. E. E. Gray, J. G. Cyster, *J. Innate Immun.* **4**, 424–436 (2012).
12. A. M. Magnuson *et al*., *Proc. Natl. Acad. Sci. U.S.A.* **112**, 1511–1516 (2015).
13. H. Yaziji, A. M. Gown, *Int. J. Surg. Pathol.* **11**, 11–15 (2003).
14. H. Stenmark, *Nat. Rev. Mol. Cell Biol.* **10**, 513–525 (2009).
15. M. Gaya *et al*., *Science* **347**, 667–672 (2015).
16. V. Cortez-Retamozo *et al*., *Proc. Natl. Acad. Sci. U.S.A.* **109**, 2491–2496 (2012).
17. R. A. Franklin *et al*., *Science* **344**, 921–925 (2014).
18. M. Iannacone *et al*., *Nature* **465**, 1079–1083 (2010).
19. W. Kastenmüller, P. Torabi-Parizi, N. Subramanian, T. Lämmermann, R. N. Germain, *Cell* **150**, 1235–1248 (2012).
20. E. A. Moseman *et al*., *Immunity* **36**, 415–426 (2012).
21. P. Andreu *et al*., *Cancer Cell* **17**, 121–134 (2010).
22. K. E. de Visser, L. V. Korets, L. M. Coussens, *Cancer Cell* **7**, 411–423 (2005).
23. P. M. Hogarth, G. A. Pietersz, *Nat. Rev. Drug Discov.* **11**, 311–331 (2012).
24. T. A. Wynn, A. Chawla, J. W. Pollard, *Nature* **496**, 445–455 (2013).
25. Y. R. Carrasco, F. D. Batista, *Immunity* **27**, 160–171 (2007).
26. T. Junt *et al*., *Nature* **450**, 110–114 (2007).
27. T. G. Phan, J. A. Green, E. E. Gray, Y. Xu, J. G. Cyster, *Nat. Immunol.* **10**, 786–793 (2009).
28. C. H. Ries, S. Hoves, M. A. Cannarile, D. Rüttinger, *Curr. Opin. Pharmacol.* **23**, 45–51 (2015).
29. K. Ohnishi *et al*., *Cancer Sci.* **104**, 1237–1244 (2013).

ACKNOWLEDGMENTS

We thank M. Ericsson for helping with electron microscopy studies, T. Murooka for multiphoton microscopy experiments, and S. Mordecai for imaging flow cytometry. The data presented in this manuscript are tabulated in the main paper and in the supplementary materials. Supported by the Samana Cay MGH Research Scholar Fund and NIH grants R21-CA190344, P50-CA86355, and R01-AI084880 (M.J.P.); NIH grants U54-CA126515, T32CA79443, RO1EB010011, 1R01CA164448, and 1R33CA202064 (R.W.); NIH grant P01-CA069246 (X.O.B. and R.W.); NIH grant U19 CA179563 (X.O.B. and T.R.M.); NIH grant R01 AI097052 (T.R.M.); NIH grant F31-CA196035 (C.G.); an EMBO long-term fellowship and an MGH ECOR Funds for Medical Discovery Fellowship (F.P.); Deutsche Forschungsgemeinschaft grant PF809/1-1 (C.P.); a Canadian Institutes of Health Research postdoctoral fellowship (C.P.L.); and Boehringer Ingelheim Funds (C.E.).

SUPPLEMENTARY MATERIALS

www.sciencemag.org/content/352/6282/242/suppl/DC1
Materials and Methods
Figs. S1 to S27
Table S1
References (*30*–*38*)

21 December 2015; accepted 25 February 2016
Published online 17 March 2016
10.1126/science.aaf1328

SCS macrophages suppress melanoma by restricting tumor-derived vesicle–B cell interactions

Ferdinando PucciChristopher GarrisCharles P. LaiAndita NewtonChristina PfirschkeCamilla EngblomDavid AlvarezMelissa SprachmanCharles EvavoldAngela MagnusonUlrich H. von AndrianKatharina GlatzXandra O. BreakefieldThorsten R. MempelRalph WeisslederMikael J. Pittet

Science, 352 (6282), • DOI: 10.1126/science.aaf1328

Macrophages block tumors' spread

Tumors constantly communicate with their surrounding tissue and the immune system. One way tumors likely do this is by secreting extracellular vesicles (tEVs), which can carry bits of the tumor to distant sites in the body. Pucci *et al.* tracked tEVs in tumor-bearing mice and people and studied how they affect cancer progression. They found that tEVs disseminate through lymph to nearby lymph nodes, where a specialized population of macrophages largely block any further travel. This barrier breaks down, however, as cancer progresses and also in the face of certain therapies. The tEVs can then penetrate lymph nodes, where they interact with B cells that promote further tumor growth.

Science, this issue p. 242